Antimicrobial properties of green synthesis of MgO micro architectures via *Limonia acidissima* fruit extract

T.B. Nijalingappa[a,b], M.K. Veeraiah[b,*], R.B. Basavaraj[c], G.P. Darshan[d], S.C. Sharma[e], H. Nagabhushana[c]

[a] Department of Chemistry, Sree Siddaganaga College of Arts, Science & Commerce, Tumkur, 572102, India
[b] Sri Siddhartha Academy of Higher Education, Tumkur, 572105, India
[c] C.N. R. Rao Center for Advanced Materials, Tumkur University, Tumkur, 572103, India
[d] Department of Physics, Acharya Institute of Graduate Studies, Bangalore, 560107, India
[e] Jain University, Jakkasandra Post, Kanakapura Taluk, Ramanagara Dist, Bengaluru, 562112, India

ABSTRACT

This paper reports a simple ecofriendly green combustion synthesis of magnesium oxide (MgO) micro architectures using various concentrations of *Limonia acidissima* fruit extract. The powder X-ray diffraction (PXRD) patterns of the as-formed product show single cubic phase and no further calcination was required. The crystallite size was obtained using Scherer's formula and was found to be 4–8 nm. The structural analysis was further analysed by Rietveld refinement technique. The morphology of combustion derived MgO micro architectures (NPs) were studied by using Scanning electron microscope. Various shaped nanostructures were obtained with different reaction parameters such as fuel concentration, pH and calcination temperatures. The Fourier transform infrared spectral studies reveal the various bond stretching in the prepared micro architectures. The growth mechanism for the formation of flower like structures were proposed. The diffuse reflectance spectral studies were carried out and energy band gap were estimated from the DRS spectra and the values ranges between (5.06–5.66 eV). Photoluminescence (PL) studies were carried upon exciting at 342 nm. A broad emission peak centered at ~399 nm and 481 nm in the bluish-violet region was recorded. The Chromaticity diagrams were studied and found that MgO NPs emit bluish-violet color. Further, the obtained NPs were investigated for their antibacterial and antifungal activity. The results indicated that MgO NPs were effectively used as good candidates for antibacterial, waste water treatment, food safety applications and biomedical markers.

1. Introduction

Nanomaterials offer auspicious opportunities for enhanced and tailored assets to use in various fields owing to their sole physicochemical properties, produced by their nanosized dimensions and large surface to volume ratios (Talebian et al., 2013). Nanomaterials are of special interest not only for basic research, but also for their interesting applications in various fields including flat panel displays, solar energy converters, optical amplifiers, electroluminescent devices, photodiodes, bio-detectors, color display, catalysts, host for solid state lasers, solid electrolytes, chemical sensors, magnetic refrigeration materials, substrates for high-temperature superconductor deposition, thermal barrier coatings, etc (Norris et al., 2008; Si et al., 2005; Yang et al., 2003; Choi et al., 2004; Medenbach et al., 2001).

Magnesium oxide (MgO) is an important wide band gap semiconductor/insulator material which crystallizes in rock salt/sodium chloride (NaCl) type cubic structure. Further, MgO is found to be extremely significant owing to its multi functional applications in water purification, catalysis, refractory, paint, luminous ceramics, and superconductor products (Zawadzki, 2008; Chavan et al., 2008 and Jin et al., 2012a,b), due to high specific surface area of MgO nanomaterials, they are found to catalyse efficiently in variety of organic reactions (Aruna and Mukasyan, 2008; Ianos and Lazau, 2009 and Umesh et al., 2012), Also it plays very important role in biological and medical applications for cancer therapy (Premkumar et al., 2013; and Krishnamoorthy et al., 2012). Various kinds of fabrication techniques are employed to synthesize MgO micro architectures such as Chemical vapour deposition (CVD) (Zawadzki, 2008), Pulsed laser deposition (PLD) (Jin et al., 2012a,b), Laser ablation (Aruna and Mukasyan, 2008), Molecular beam epitaxy (MBE) sputtering method (Chen et al., 2004),

Table 1

Calcination temperature and surface morphology of MgO by different authors.

Sl. No	Sample	Preparation technique	Structural morphology	Calcination/Annealing temperature (°C)	Reference
1	MgO	Bio template	Conical, nanoflowers	500	Present work
2	MgO	sol-gel	–	500	Hakimeh et al., [31]
3	MgO	Template-free reflux condensation approach	cubic	–	Mageshwari et al., [32]
4	MgO	spray pyrolysis technique	cubic	573	Nemade et al., [33]
5	MgO	ultrasound	cubic	600	Safaei-Ghomi et al., [34]

Table 2

Main composition of fruit extract of *L. acidissima*.

Main composition[b]	Concentration (%)
Moisture	85 ± 0.51[a]
Lipid	29 ± 0.1
Carbohydrates	42.2 ± 0.2
Protein	3.19 ± 0.7
Crude fibre	11.52 ± 0.4
Ash	8.5 ± 0.3

[a] Values are mean $\pm$ standard deviation of three replicates.
[b] AOAC.

Table 3

Amino acid composition of fruit *L. acidissima*.

Amino acid composition	Concentration (mg/100 g dry weight)
Aspartic acid	104.16
Glutamic acid	Negligible
Alanine	169.82
Methionine	Negligible
Tyrosine	605.19
Lysine	Negligible
Threonine	Negligible
Proline	939.04
Isoleucine	2870.41
Phenylalanine	984.15
Trytophan	1154.51
Serine	Negligible
Glycine	152.23
Valine	471.53
Leucine	176.06
Histidine	414.95
Arginine	206.49

hydrothermal method (Yang and Kim, 2004), Sol-gel method (Han et al., 2004), Co-precipitation method (Wegner and Pratsinis, 2005) and Thermal decomposition of hydroxide or carbonate (Granados-Correa at al., 2008; Tamilselvi et al., 2013).

However, these preparation methods are expensive and involve complex procedures, sophisticated equipments, and the use of environmentally malignant chemicals and organic solvents which were toxic and not easily degraded in the environment. Thus, developing a simple green synthetic process for preparing MgO micro architectures is of interest.

Solution combustion synthesis (SCS) is known for a simple and easier for the synthesis of metal oxide nanomaterials. It is an energy saving process and produces nanomaterials within 5 min. Here metal nitrates in general and *Limonia acidissima* fruit extract as a fuel is dissolved in water to get homogeneous solution. i.e, it ensures the uniform distribution at atomic level mixing and produces ultrafine powder with reduced particle size. Again, the role of combustible fuel is very important as it is responsible for the liberation of energy to produce fluffy mass in combustion method. Granados - Correa et al. and Sunandana et al. Synthesized MgO powders via a solution combustion process using urea as fuel (Alhaji et al., 2017; Nassar et al., 2017). Balamurugan et al. synthesized MgO micro architectures via combustion method using hexamine as fuel (Vasanthia et al., 2017). Kaviyarasu et al. synthesized MgO micro architectures using glycine as fuel and studied its dielectric properties (Kaviyarasu and Devarajan, 2011), Bai et al. synthesized MgO micro architectures using starch as fuel (Bai et al., 2011).

Quite different from the conventional approaches, many researchers have used naturally occurring compounds as a combustible fuel for the preparation of nanocrystalline metal oxides (Jeevanandam et al., 2017; Mageshwari et al., 2013; Cai et al., 2017; Sushma et al., 2016; Srivastava et al., 2015). To the best our knowledge, we have not found any article for the synthesis MgO micro architectures via solution chemistry route. *Limonia acidissima* fruit extract employed as fuel as a reducing agent instead of using chemicals. Table 1. Shows the literature review on different preparation techniques and surface morphology of MgO.

2. Experimental

2.1. Extraction of Limonia acidissima fruit

The *Limonia acidissima* pulp was collected from Tumkur University campus India and washed several times in running tap water followed by distilled water for 3–4 times and then shaded dried at room temperature for 10 days. After shaded dried plant material then powdered mechanically using electric pulvizer and sieved, (sieve No.10/44) stored in an airtight container separately. The shade dried, powdered materials (100 g) were subjected to successive deionized water and kept in reflect for 5 h and obtained solution was filtered. The filterate solution and concentrated in vacuum using rotary flash evaporator. Left over solvent was completely removed on water bath and finally dried in the desiccators. Finally crude extract was obtained and stored in container further analysis. The major composition of fruit *L. acidissima* was given in Table 2. The amino acid composition of *L. acidissima* was given in Table 3 (Priya Darsini et al., 2016).

2.2. Green synthesis of MgO nanostructures

2 gm of Magnesium nitrate [Mg $(NO3)_2$. (99.9%)] and 5 gm *Limonia acidissima* fruit extract was dissolved in double distilled water in a Pyrex dish and then mixed uniformly using magnetic stirrer for 5 min. Thereafter, the Pyrex dish was introduced in a pre-heated muffle furnace maintained at a temperature of $300 \pm 5\,°C$. The obtained product is calcined at $500\,°C$ for 3 h and used for characterization. The schematic diagram used for green combustion synthesis was shown in Fig. 1.

2.3. Characterization

Shimadzu 7000 (Cu-Kα radiation with nickel filter, $\lambda = 0.15406$ nm) was utilized to study the structural characterization. Hitachi- TM 3000 and Hitachi H-8100, Kevex sigma TM Quasar, USA
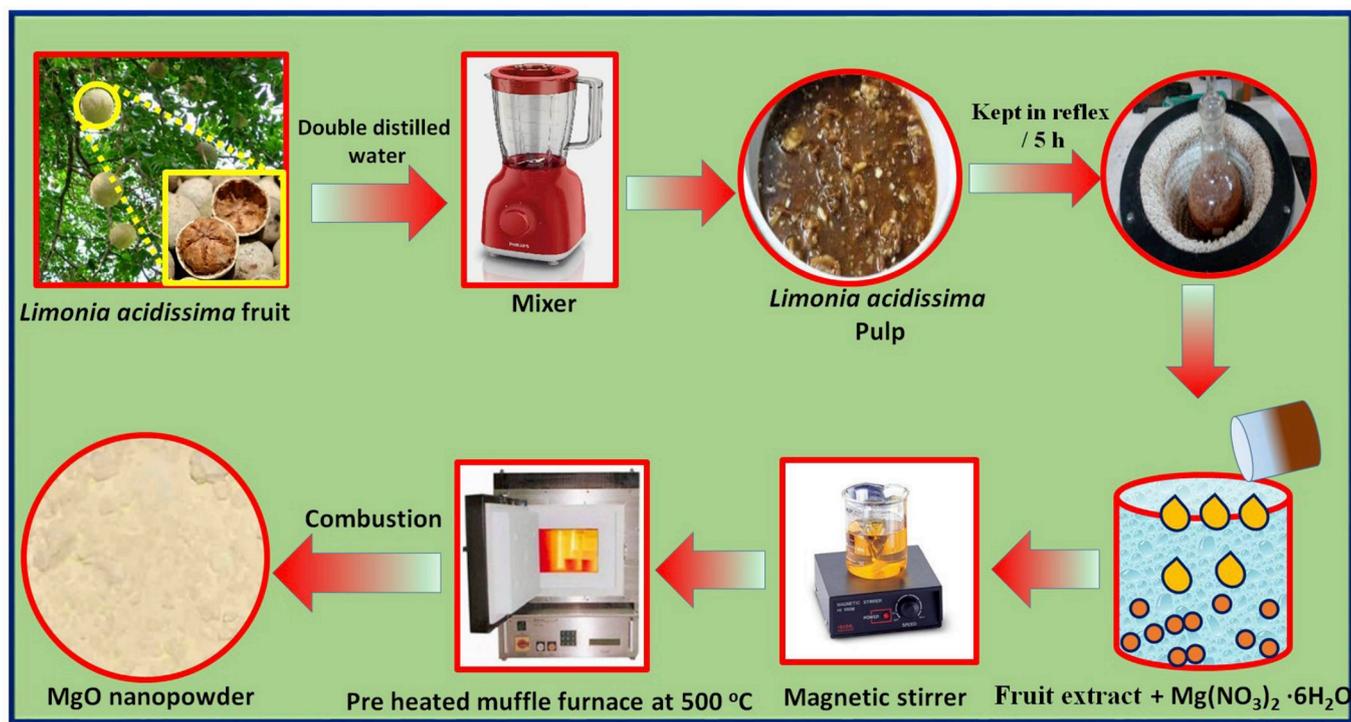
Fig. 1. Schematic illustration of green synthesis of MgO NPs using *Limonia acidissima* fruit extract. (For interpretation of the references to color in this figure legend, the reader is referred to the Web version of this article.)

Table 4
Bacterial isolates used for evaluation of MgO micro architectures antibacterial activity.

Gram reaction grouping	Bacterial Strain	Isolate Number
Gram Negative	*Escherichia coli*	ATCC 8739
Gram Negative	*Klebsiella pneumoniae*	ATCC 13883
Gram Negative	*Pseudomonas aerguinosa*	ATCC 9027
Gram Positive	*Staphylococcus aureus*	ATCC 6538

were used for SEM and TEM analysis. Lambda – 35, PerkinElmer was used to record the diffuse reflectance spectra. Horiba Spectroflourimeter (Jobin Yvon) was utilized to study the photoluminescence measuremenst.

2.4. Antibacterial studies of bioengineered magnesium oxide (MgO) micro architectures bacterial strains, culture conditions and supplements

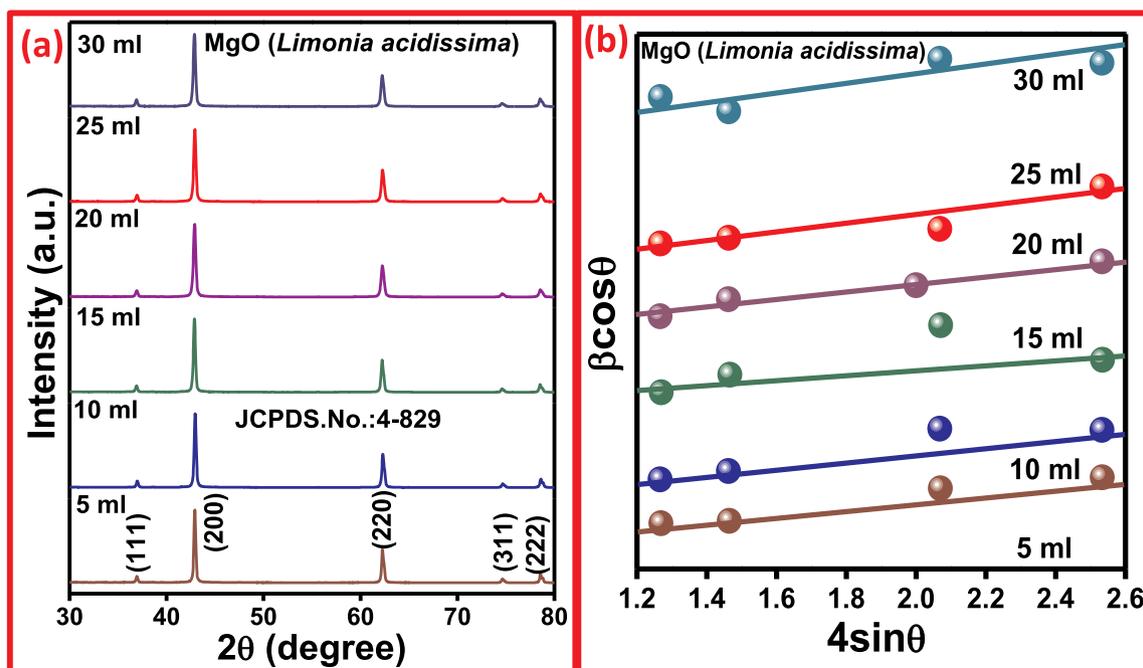American Type Culture Collection (ATCC) registered standard and

Fig. 2. (a) PXRD profiles and (b) Williamson-Hall plots of MgO micro architectures.

Table 5
Estimated the crystallite size, strain, stacking fault and dislocation density values of the asformed MgO nano particles.

Sample	Fuel Conc. (ml)	Crystallite Size (nm)		Strain 10^{-3}	Stacking fault	Dislocation density (δ)	Energy gap (E_g) in eV
		Debye Scherer's	W−H plot				
As-formed	5	8	11	11.70	0.4405	5.7307	5.06
	10	6	7	10.76	0.4418	6.2771	5.37
	15	5	8	3.09	0.4414	1.9747	5.50
	20	6	7	3.64	0.4412	1.4986	5.56
	25	8	6	3.80	0.4423	2.4282	5.61
	30	4	5	3.23	0.4417	4.9163	5.66

clinical strain isolates were obtained from American Type Culture Collection Centre, USA were used in this present research work (Table 4). Except stated or else strains were grown in Mueller-Hinton (MH) broth with aeration at 37 °C. Bacterial strains were preserved on agar plates of their respective medium and were stored at -80 °C in 20% glycerol for long-term preservation. If required, streptomycin was used with a final concentration of 100 g/ml.

All the above listed four bacteria were cultivated on Mueller-Hinton agar (Hi-Media, Mumbai, India) and were incubated at 37 °C for 24 h in aerobic environments. A single colony from the stock bacterial Petriplates were used for preparing bacterial suspensions separately. A loop full of inoculum from bacterial culture was inoculated to 20 ml of sterile Mueller-Hinton broth in 100 ml Erlenmeyer flask. These flasks were kept in an agitator for 24 ± 2 h at 200 rpm with 37 °C. Subsequently, an optical density McFarland of 0.5 (1×10^8 CFU/ml) was made separately with isotonic solution (NaCl− 0.85%). These bacterial suspension was diluted ten times (1×10^7 CFU/mL) individually and used as inoculum for bactericidal activity measurement. Inhibition action of bacteria was examined in broth medium containing a range of concentrations (0.0, 0.0025, 0.025, 0.25, 2.5 and 25 μg/ml) of magnesium oxide micro architectures.

2.5. Antibacterial assessment by minimum inhibitory concentration (MIC) and minimum bactericidal concentration (MBC) of magnesium oxide micro architectures through microbroth dilution technique

The effect of magnesium oxide micro architectures on the growth of *E. coli, Klebsiella pneumoniae, P. aeruginosa* and *S. aureus* was determined by microbroth dilution method with treated and untreated bacterium. Growth inhibition of bacteria was examined in broth medium encompassing a range of MgO micro architectures (MgO NPs) concentrations (0.0, 0.0025, 0.025, 0.25, 2.5 and 25 μg/ml). Cells of *E. coli, Klebsiella pneumoniae, P. aeruginosa* and *S. aureus* from advanced logarithmic growth phase were inoculated (20.0 μL) to Mueller-Hinton broth in microtitre wells. The MIC was determined by adopting with slight substitution. MgO micro architectures stock suspension was prepared by suspending the micro architectures in milli-Q water to achieve a concentration of 100 μg/mL. Then the aliquot was subjected to sonication and the suspension later mixed with Mueller-Hinton broth for use in the subsequent experiments. The above mentioned four bacterial strains were exposed for 24 h to MgO NPs ranging from 25 to 0.0025 μg/mL in ten-fold dilution series. The parallel protocol was employed for determination of MIC by tetracycline at 25 μg/mL (positive) and sterile Mueller-Hinton broth (negative-without micro architectures) controls. Twenty μL of the bacterial suspension (10^7 CFU/mL) was added to each microtitre well and incubated at 37 °C for 24 h. The experiments were repeated times in triplicates. Later, minimum inhibitory concentration values of the micro architectures were revealed by adding 25 μL, iodonitrotetrazolium chloride (INT at 0.5 mg/

mL) in each well after 24 h. Microtiter plates were further incubated at 37 °C for 60 min. MICs of test compounds were determined as the lowest micro architectures concentration that constrained the color change from colorless to red due to absence of bacterial growth. From theses microtiter wells, MBC was determined by transferring 50 μL bacterial suspension (absence of INT) on Mueller-Hinton (MH) agar in Petriplates by streak inoculation within divided sector. Such Petriplates were nurtured for 24 h at 37 °C. Minimum bactericidal concentration was the lowest concentration that completely exterminate the bacterial growth on MH agar Petriplates.

2.6. Antifungal studies of bioengineered MgO micro architectures through food poison technique

Fungal organism's *viz.*, *Alternaria alternata* (causing leaf spot and early blight of tomato) and *Phomopsis azadirachtae* (causing die-back disease of neem) with the courtesy of culture collection Centre of the Molecular Diagnostics Laboratory, Department of Microbiology and Biotechnology at the Bangalore University, Bangalore, India was considered for antifungal evaluation by the food poison technique (Lakshmeesha et al., 2014) with slight adjustments. *Alternaria alternata* and *Phomopsis azadirachtae* were grown on malt extract agar (MEA) at 25 ± 1 °C and maintained with 12 h alternate dark and light cycle. The sterilized MEA media added with bioengineered MgO NPs at concentrations of 100, 200, 300, 400, 500, 600 and 700 μg/mL and the MEA medium without MgO micro architectures (negative control) were used. The antifungal property of MgO micro architectures was compared with traditional antifungal agent bavistin (positive control). The MEA media were inoculated with the pathogenic fungal organisms as 5 mm diameter mycelial-agar-disc that are prepared aseptically from the seven-day-old culture margin. These mycelial-agar-disc was inoculated to each Petri dish on different concentrations of bioengineered MgO NPs and controls media (positive and negative controls). Both MgO micro architectures amended and the control Petri dishes were kept in an incubator at 25 ± 1 °C for seven days. The antifungal activities of MgO NPs on two pathogenic fungi was measured by means of radial growth in mm. All the tests were executed in triplicate with three times repetition. The percent inhibition of fungal growth by MgO NPs was calculated as cited underneath:

$$\text{Percent inhibition of fungal growth} = \left[\frac{dc-dt}{dc} \right] x 100 \tag{1}$$

Wherever, d_c is the average increase in mycelial growth in control treatment and dt is the average increase in mycelial growth in treatment.
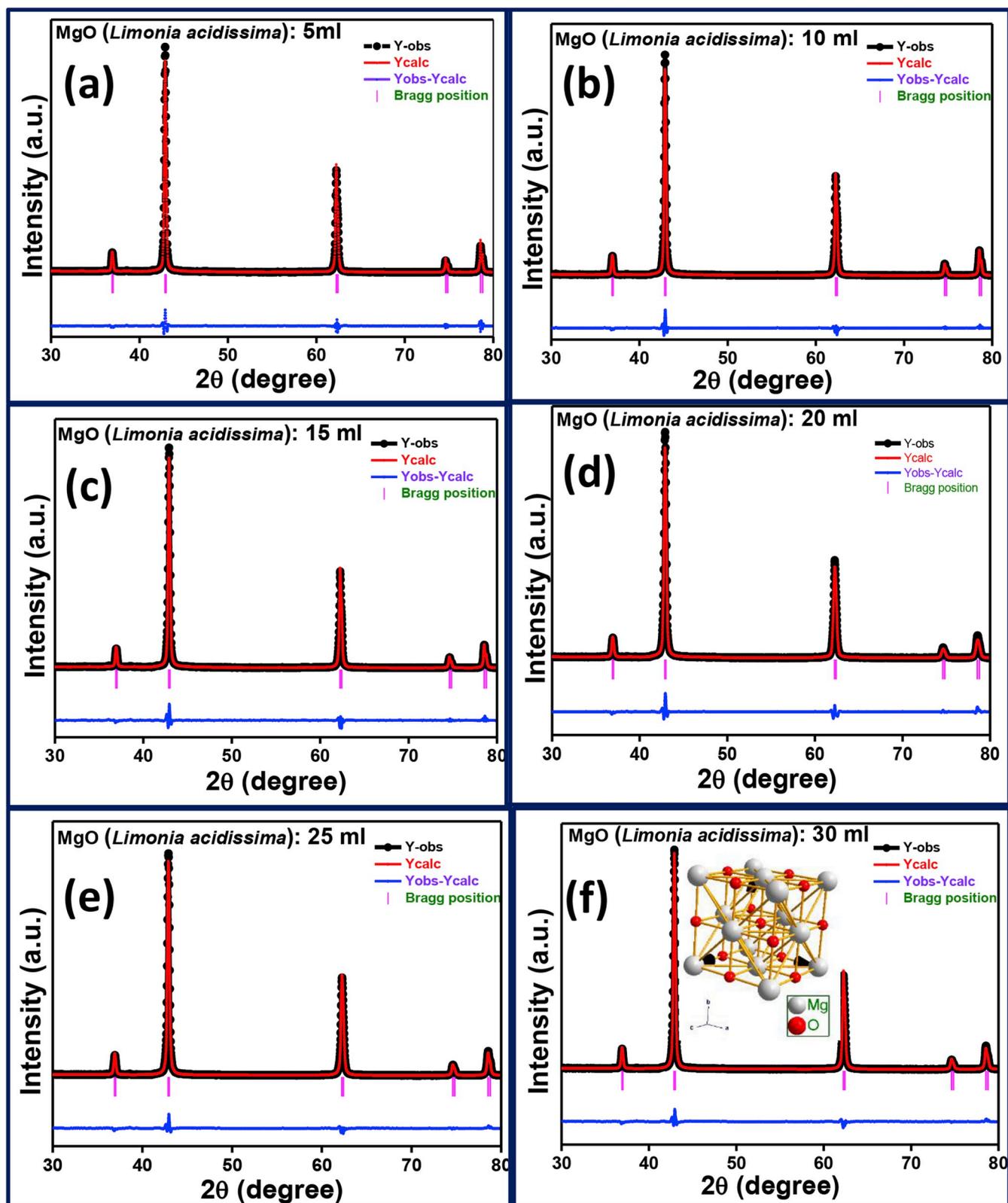
Fig. 3. Rietveld refinement of MgO prepared with different concentrations (a) 5 ml, (b) 10 ml, (c) 15 ml, (d) 20 ml, (e) 25 ml and (f) 30 ml (Inset: packing diagram) of *Limonia acidissima* fruit extract.

Table 6
Rietveld refined structural parameters of MgO NPs.

Compound	5 ml	10 ml	15 ml	20 ml	25 ml	30 ml
Crystal system	Cubic	Cubic	Cubic	Cubic	Cubic	Cubic
Space group	Fm 3 m (225)	Fm 3 m (225)	Fm 3 m (225)	Fm 3 m (225)	Fm 3 m (225)	Fm 3 m (225)
Lattice parameters (A°)						
a = b = c	4.2147	4.2152	4.2149	4.2152	4.2157	4.2147
α = β = λ	90°	90°	90°	90°	90°	90°
Unit cell volume (A°^{3})	74.8674	74.8950	74.8775	74.8960	74.9212	74.8689
Atomic coordinates						
Mg						
x	0.00000	0.00000	0.00000	0.00000	0.00000	0.00000
y	0.00000	0.00000	0.00000	0.00000	0.00000	0.00000
z	0.00000	0.00000	0.00000	0.00000	0.00000	0.00000
O						
x	0.50000	0.50000	0.50000	0.50000	0.50000	0.50000
y	0.50000	0.50000	0.50000	0.50000	0.50000	0.50000
z	0.50000	0.50000	0.50000	0.50000	0.50000	0.50000
Refinement parameters						
R$_P$	5.97	5.46	5.72	5.88	5.80	5.92
R$_{WP}$	7.70	6.83	7.38	7.46	7.50	7.52
R$_{Exp}$	7.23	7.36	7.39	7.38	7.41	7.57
χ^2	1.13	0.86	0.99	1.02	1.02	0.99
GoF	1.10	0.92	0.99	1.00	1.00	0.99
R$_{Bragg}$	2.21	2.67	2.90	2.66	2.53	2.54
R$_F$	1.44	1.60	1.83	1.77	1.47	1.52
X-ray density (g/cc^3)	3.576	3.575	3.575	3.574	3.573	3.576

2.7. Statistical analysis

The antifungal experimental data was analysed by mean ± SD subjected to multivariate analysis. Means are separated by Duncan's multiple range test at 0.5 significance ($P < 0.05$) using SPSS software (version 19).

3. Results and discussion

3.1. Structural analysis

Fig. 2a shows the Powder X-ray diffraction patterns of MgO NPs prepared via solution combustion route using *Limonia acidissima* (La) fruit extract as fuel. It was observed from the figure that all the diffraction peaks were well matched with the cubic phase with standard JCPDS.No: 4–829 and belongs to the space group Fm-3m (no. 225) (Devaraja et al., 2016). The peaks at the diffraction angles of 36.90, 42.82, 62.27, 74.80 and 78.21 are attributed to (111), (200), (220), (311) and (222) planes, respectively. The diffraction patterns were recorded for various concentrations (5–30 ml) of the fruit extract.

The average crystallite size of prepared samples were estimated by using Debye Scherrer's relation,

$$D = 0.9\lambda/\beta \cos\theta \tag{2}$$

where λ; the wavelength of the X-rays, β; the full-width at half maximum (FWHM) and θ; the angle of diffraction. The average crystallite size of MgO NPs were estimated and listed in Table 5. The broadening of PXRD peaks were mainly related to estimate the crystallite size or strain present in the samples. Williamson – Hall (W - H) fitting equation was used to estimate the crystallite size and lattice micro – strain present prepared samples was expressed as (Nagabhushana et al., 2016):

$$\beta\cos\theta = \varepsilon(4\sin\theta) + \frac{\lambda}{D} \tag{3}$$

where '*β*' (FWHM in radians) was measured for different PXRD lines corresponding to different planes, *ε*; the strain developed, *D*; the crystallite size and θ; Bragg's diffraction angle. The crystallite size and micro – strain were estimated and tabulated in Table 5. The W−H plots were shown in Fig. 2b.

The other structural parameters such as dislocation density (δ) and stacking fault (SF) were evaluated by using following relations (Basavaraj et al., 2017a,b,c):

$$\delta = \frac{1}{D^2} \tag{4}$$

$$SF = \left[\frac{2\pi^2}{45(3\tan\theta)^{1/2}}\right] \tag{5}$$

The estimated dislocation density and stacking fault were given in Table 5. The cubic structure of the prepared samples was confirmed through structural Rietveld refinement by using *Fullprof Program*. The results were in good agreement with observed and calculated PXRD patterns (Fig. 3). The structural refinement quality was measured by a parameter called goodness of fit (GoF). In the present work, estimated GoF was found to be ~ 0.73. The packing diagram of prepared MgO NPs by utilizing diamond software was shown in inset Fig. 3 (f). The obtained reitveld refined parameters were tabulated in Table 6.

3.2. Diffuse reflectance spectral studies

The optical properties of nanostructures were studied by means of diffuse reflectance spectroscopy (Fig. 4a). The spectra were recorded in the range of 200–1100 nm wavelength region at room temperature. It
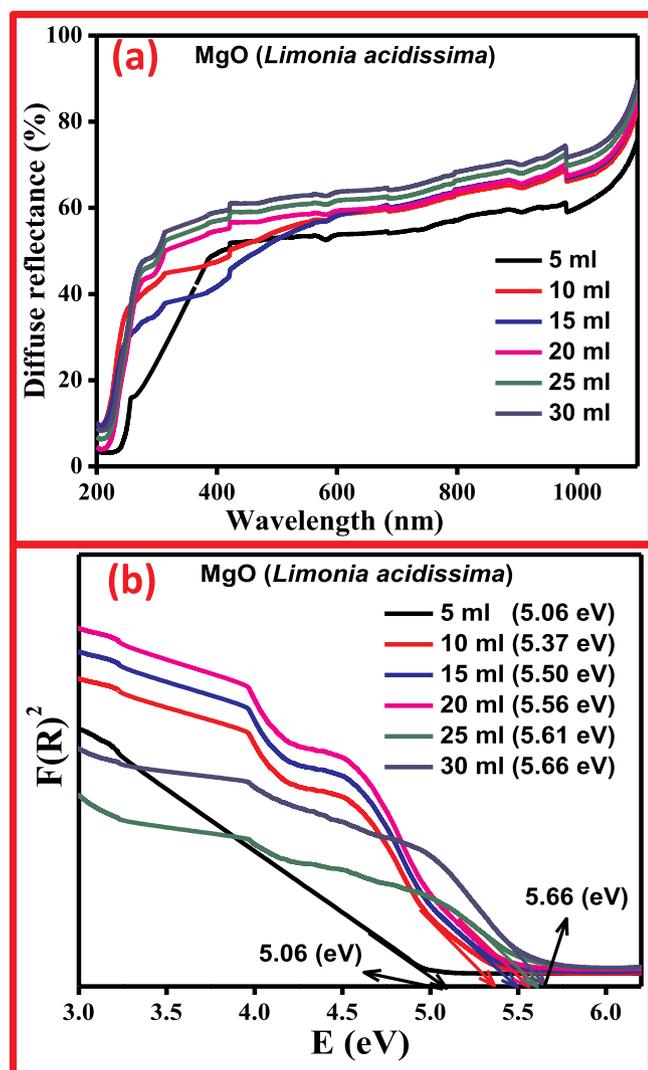
Fig. 4. (a) Diffuse reflectance spectra and (b) energy band gap plots of MgO micro architectures.

can be seen from Fig. 4 (a) that a strong absorption peak observed from 350 to 400 nm.

To determine the energy band gap, Kubelka –Munk function was used. The Kubelka–Munk function F (R_∞) and band gap energy ($h\nu$) were estimated by utilizing the following equations:

$$F(R_\infty) = \frac{(1 - R_\infty)^2}{2R_\infty} \tag{6}$$

$$h\nu = \frac{1240}{\lambda} \tag{7}$$

where R_∞; reflection coefficient of the sample, λ; the absorption wavelength. The energy band gap values were evaluated and were summarized in Table 2 (Ramakrishna et al., 2016). Fig. 4b shows the energy band gap (Eg) values of as-formed MgO was found to be in the range of 3.24–3.69 eV and that for calcined sample it was found to be around 2.86–3.20 eV, which was much lesser than the as-formed MgO which means increase in oxygen vacancy in the sample. Therefore, which gives the evidence for the quantum confinement of calcined

MgO (Devaraja et al., 2014a,b). From Table 5, we can also observe the reason for the varied band gap with respect to the different fuel concentration.

3.3. Morphological analysis

The various reaction parametres reveals effect of concnetrations of fruit extract (5, 10, 20 and 30 ml), pH (1, 3, 5 and 9) and temperatures (500, 600, 700 and 800 °C) on the morphology of the product was studied. Fig. 5 shows the SEM micrographs of MgO nanostructures prepared with different concentrations of *Limonia acidissima* fruit extract. A drastic change in the morphology was observed for the different concentration of the fuel. A complete flower like morphology was obtained for 30 ml fo the fruit extract (Fig. 5d). The pausible growth mechanism for the formation of flower like morphology of the MgO nanostructures was shown in Fig. 6. Also the trapping of MgO NSs in the Isoleusine frame network was illustrated with the egg box model as shown in Fig. 7.

The effect of pH value on the morphology was also studied in detail. Fig. 8 depicts the SEM mcirographs of MgO NPs prepared with different pH values (1, 3, 5 and 9) under 30 ml of the fruit extract. It can be observed from the figure that at initial pH value of a and 3 the particles were in aglglomerated in nature and connected with one another (Fig. 8a and b). As the pH concentration was increased to 5 and 9 the morphology was further changed from agglomeration to well spherical in shape (Fig. 8d). The results indicated that the change in pH value will effect the morphology of the product.

The effect of calcination temperature on the morphology was also studied in detail. Fig. 9 depicts the SEM microgrpahs of MgO NPs calcinated for different temperatures (500, 600, 700 and 800 °C) under 30 ml of the fruit extract. It can be observed from the figure that the particles were formed in flake like structures and this flake like morphology increased with the increase in calcination temperature from 500 to 800 °C (Fig. 9 a-d).

The particle size was further estimated by the TEM analysis. Fig. 10 shows the TEM, HRTEM and SAED patterns of MgO NPs prepared under 500 °C with 30 ml of fruit extract. From Fig. 10a it can be observed that the particles were in agglomeration in nature and the size was found to be around ~10–15 nm which was in good agreement with the PXRD results. Fig. 10b, d shows the HRTEM image showing the interplanar distance (d) value ranging in between 0.28 and 0.32 nm. Fig. 10c depicts the SAED patterns of the MgO NPs showing the crystallinity of the product.

3.4. Photoluminescence (PL) studies

Fig. 11 shows PL studies of MgO NSs fabricated via solution combustion route recorded at RT at an excitation wavelength of 342 nm. The spectra exhibit an intense emission peaks at 399 nm ($^2T_{1u} \rightarrow {}^2A_{1g}$) and 481 nm ($^3B_{1u} \rightarrow {}^1A_g$) respectively (Jin et al., 2012a,b; Dixit et al., 2015; Kiran et al., 2017). Further, these peaks were arised due to surface defects (oxygen vacancies: F-centres and F^+-centres:oxygen ion vacancy occupied by single electrons). The obtained values were well compared to those obtained in the reported literature (Devaraja et al., 2014a,b). Generally oxide nanostructures exhibit more oxygen defects as well as appreciable bond breaking owing to large surface to volume ratio.

To access the quality of the phosphor material Commission International de I'Eclairage (CIE) 1931 color coordinates were studied in detail and shown in Fig. 12 (a). As can be seen from the figure the coordinates clearly located in the bulish-green region. Further, to ascertain technical applicability of prepared phosphor, CCT was
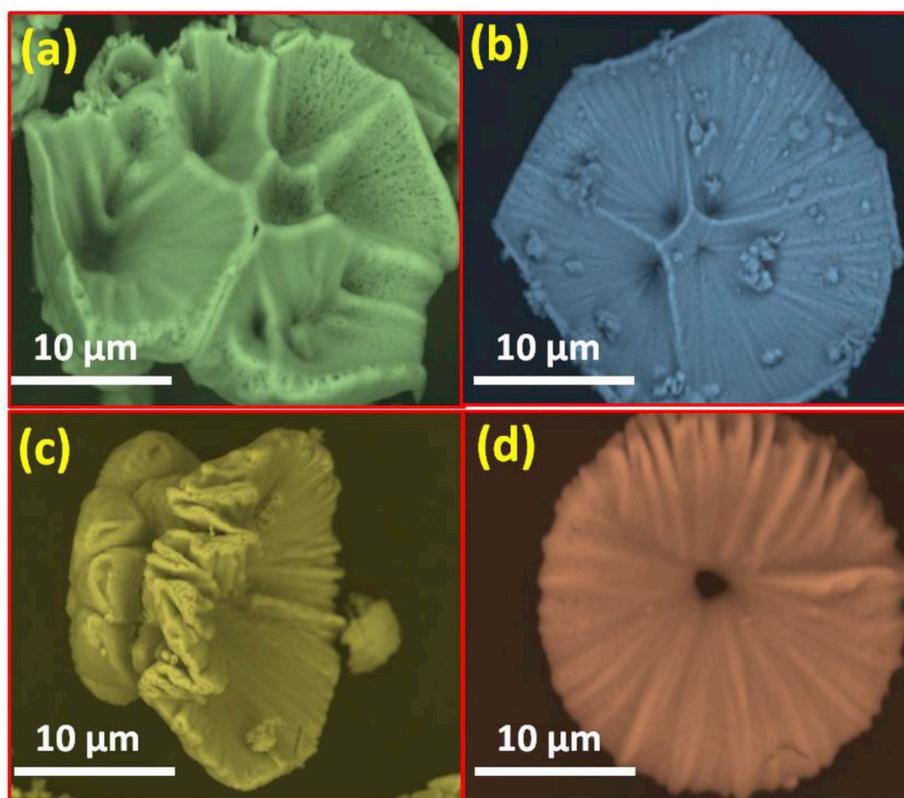
Fig. 5. SEM micrographs of MgO NPs prepared with different concentration of *Limonia acidissima* fruit extract (a) 5 ml, (b) 10 ml, (c) 20 ml and (d) 30 ml.
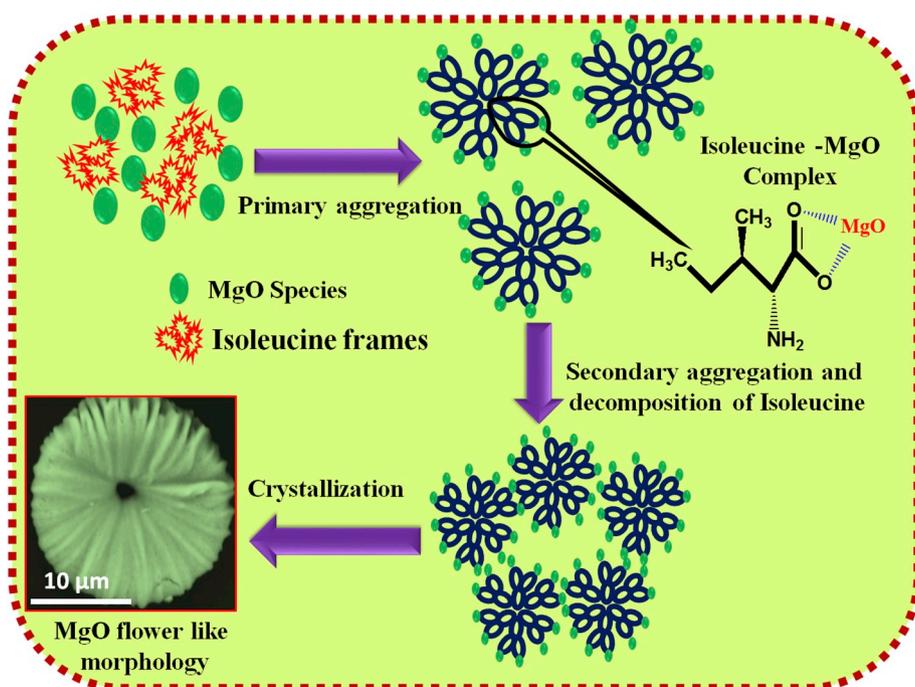

Fig. 6. Schematic illustration of growth mechanism for the formation of flower like morphology of MgO nanostructures in the presence of Isoleucine amino acid network.

estiamted (Basavaraj et al., 2017a,b,c) from CIE coordinates as shown in Fig. 12 (b). The estimated CCT value was found to ~11289 K which is greater than 5000 K as a result the phosphor was quite useful for cool LEDs.

3.5. Antibacterial studies of bioengineered magnesium oxide (MgO) micro architectures(NPs)

Minimum inhibitory concentration and minimum bactericidal concentration of all the synthesized MgO NPs with four bacteria are recorded in Table 7. MgO micro architectures displayed significant
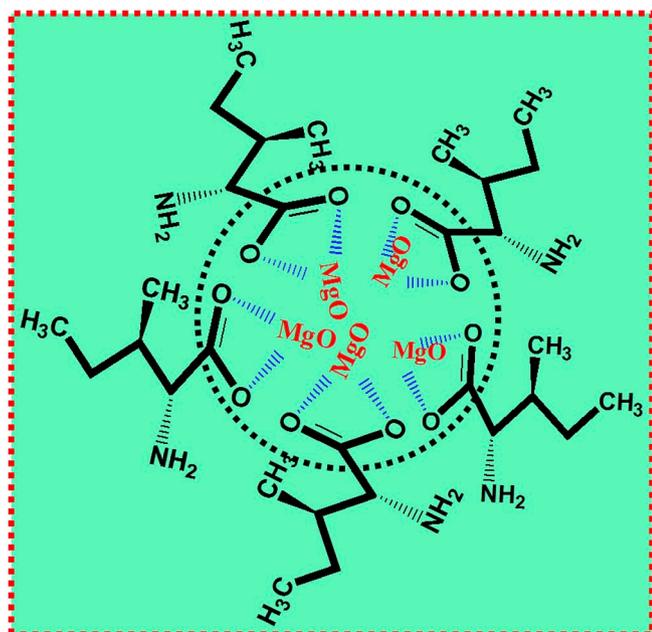
Fig. 7. Egg box model showing the trapped MgO NSs under amino acid *Isoleucine* network.

inhibition for *E. coli* was 0.25 μg/mL of micro architectures prepared with 10, 15 and 20 ml of plant extract and 2.5 μg/mL with 5 ml of plant extract (Table 7). Least MIC was 0.025 μg/mL for *K. pneumoniae*, 0.25 μg/mL for *P. aeurginosa* with distinct differences in the susceptibility to micro architectures in a dose-dependent manner (Fig. 13).

MICs observed for Gram-positive bacteria, *Staphylococcus aureus* with 0.025 μg/mL (Table 7). In Gram-negative bacteria, MgO NPs presented a MIC 0.025 μg/mL for *K. pneumoniae* (the lowest observed in the Gram-negative bacteria) and lowermost concentration in the Gram-positive *Staphylococcus aureus* was 0.025 μg/mL with micro architectures prepared with 5 ml of plant extract, it also presenting a higher potency compared to all other concentrations (Table 7).

MBC test recorded for four bacteria; *K. pneumonia* and *Staphylococcus aureus* was at 0.25 μg/mL; *P. aeruginosa* was at 2.5 μg/mL and *E. coli* was at 25 μg/mL showed a higher susceptibility to MgO micro architectures prepared with 5 ml concentration of *Limonia acidissima fruit* extract. The antibacterial effects of MgO micro architectures on gram positive bacteria are stronger than gram negative bacteria, whereas *K. pneumonia* and *Staphylococcus aureus* were more sensitive to MgO NPs as compared to *E. coli* and *Pseudomonas aeruginosa* among the four tested bacterial strains. Fully organized, these results advocate that MgO micro architectures can be employed as an antibacterial material against a broad spectrum of pathogenic bacteria.

3.6. Antifungal studies of bioengineered MgO micro architectures

In the present research communication the usage of MgO micro architectures as possible antifungal compounds was investigated. Figs. 14 and 15 shows the effective inhibition of fungal growth for both *Alternaria alternata* and *Phomopsis azadirachtae* by MgO micro architectures suspension. The average growth of *Alternaria alternata* was inhibited by 91.48% and *Phomopsis azadirachtae* by 95.33% in terms of colony growth diameters as the concentration of MgO micro architectures increased from 100 to 700 μg/mL (Table 7). The data suggest that significantly much higher difference was found for different concentrations of MgO micro architectures treatment ($P < 0.05$). These results indicate that MgO micro architectures at concentration greater
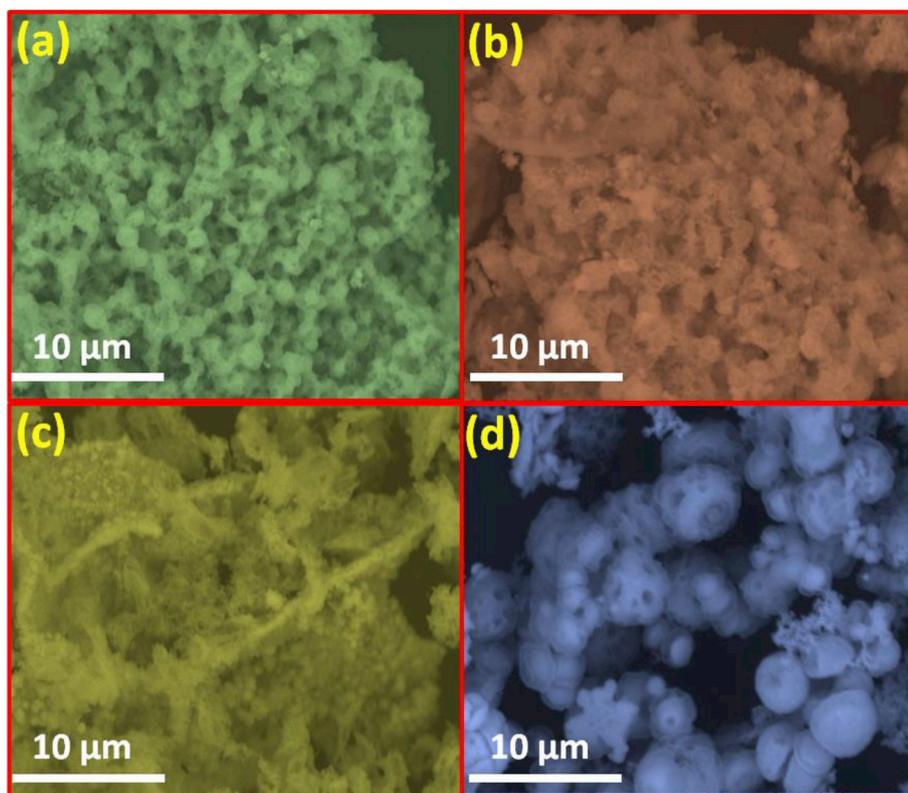

Fig. 8. SEM micrographs of MgO NPs prepared with different pH values (a) 1, (b) 3, (c) 5 and (d) 9 with 30 ml of fruit extract.
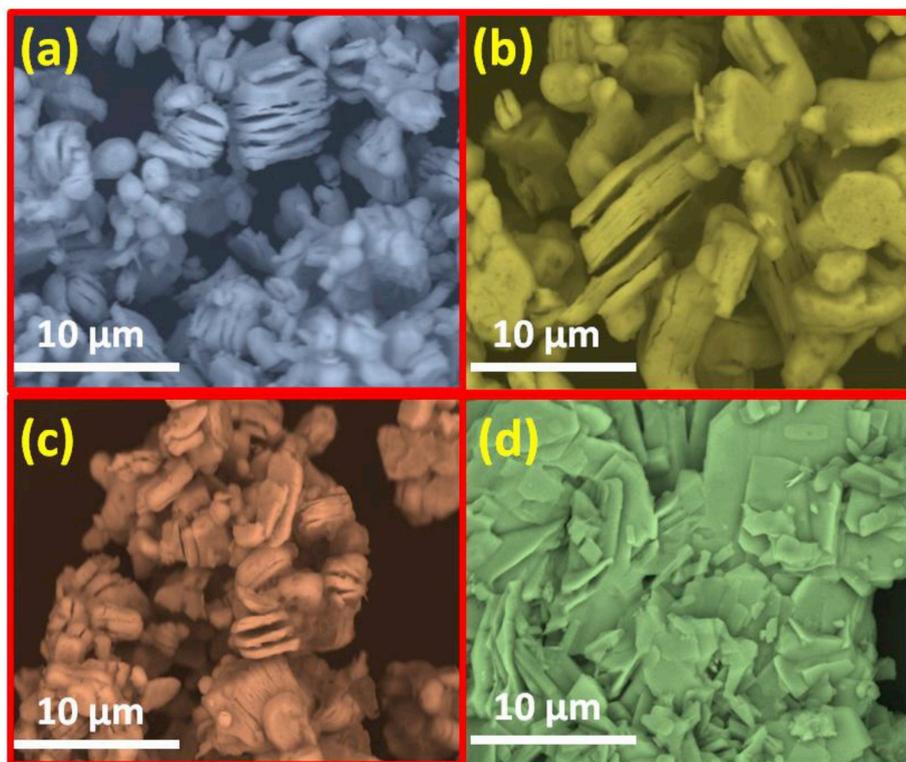
Fig. 9. SEM micrographs of MgO NPs prepared with different calcination temperatures (a) 500 °C, (b) 600 °C, (c) 700 °C and (d) 800 °C with 30 ml of fruit extract.
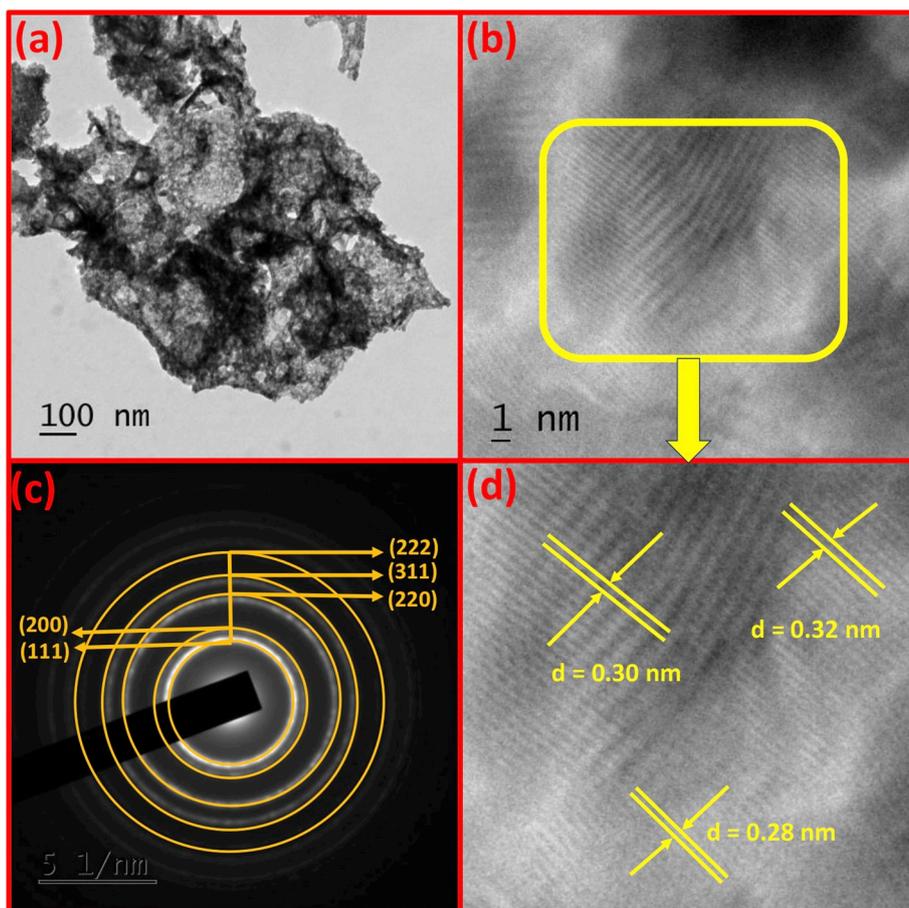

Fig. 10. (a) TEM image, (b) HRTEM and (c) SAED patterns of MgO NPs prepared with 30 ml of fruit extract at 500 °C, (d: magnified HRTEM image).
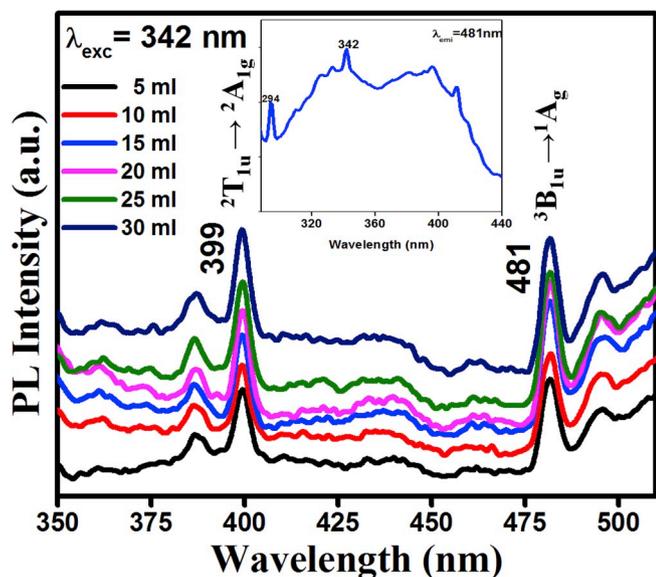
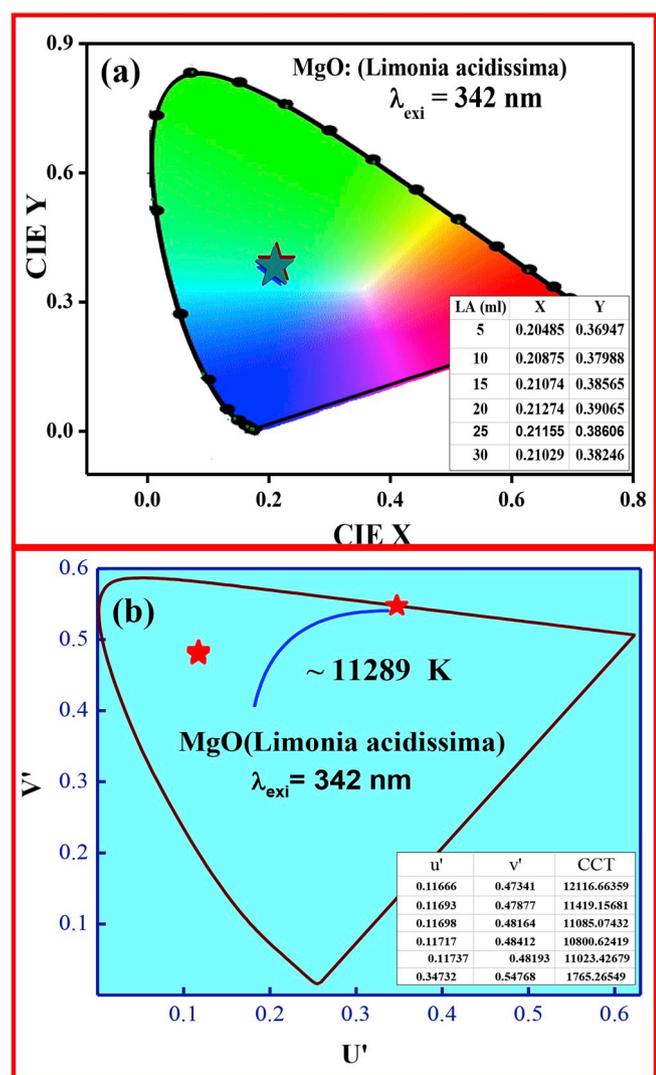**Fig. 11.** PL emission spectra of MgO NPs (Inset: excitation spectrum of MgO NPs) excited at 342 nm.

Fig. 12. (a) CIE and (b) CCT diagrams of MgO nanostrutcutres.

Table 7

Minimum inhibitory concentration and minimum bactericidal concentration of magnesium oxide micro architectures against *Staphylococcus aureus*, *Klebsiella pneumoniae*, *Escherichia coli* and *Pseudomonas aeruginosa* expressed as µg/ml.

Plant extract	5 ml		10 ml		15 ml		20 ml	
Bacterial strain	MIC	MBC	MIC	MBC	MIC	MBC	MIC	MBC
Escherichia coli	2.5	25	0.25	2.5	0.25	2.5	0.25	2.5
Klebsiella pneumoniae	0.025	0.25	2.5	25	0.025	0.25	0.25	2.5
Pseudomonas aeruginosa	0.25	2.5	2.5	25	0.25	2.5	0.25	2.5
Staphylococcus aureus	0.025	0.25	0.25	2.5	0.25	2.5	2.5	25

than 700 µg/mL can effectively inhibit *Alternaria alternata* and *Phomopsis azadirachtae* radial growth. In the present study, the micro architectures thus biosynthesized possibly will also be applied as selective antifungal agents. Fig. 16 shows the multifarious mechanism of bioengineered magnesium oxide micro architectures induced toxicity on pathogenic bacteria.

Microbicidal activities of the numerous inorganic micro architectures such as various metallic and semiconductor NPs viz., Cu, Fe, Pd, Ru, PbS, CdS, CuO, CeO$_2$, Fe$_3$O$_4$, TiO$_2$ and ZnO NPs with an emphasis on their applications in drug development were inspected distinctly or combined with biopolymer in earlier studies (Mirhosseini, 2016). Thus, it stimulated our research group for production of bio-micro architectures that leads to controlling of bacterial and fungal to protect human and plant adeptly, inexpensive and biodegradable manner. This led us to focus on MgO NPs that are low-cost, stable and sensitive to clinical pathogenic strains and phytopathogenic fungi. Moreover, it was found out that with the increase in MgO micro architectures, the antimicrobial property is increased and growth of the bacteria and fungi is decreased. Bestowing to our acquaintance, this is the only study investigating the effect of MgO micro architectures on plant pathogenic fungi. Specific studies investigated the effect of MgO micro architectures against *Candida albicans*, but they had not shown significant anti-*C. albicans* properties.

All through the past 30 years, growing incidences of the emergence and spread of antibiotic-resistant bacterial pathogens developed a health care problem worldwide. Amongst the novel drug agents employed as antimicrobials, micro architectures are under extraordinary consideration. Although, the exact antibacterial mechanism of MgO micro architectures is not clear, three main antibacterial mechanisms have been proposed, such as the formation of ROS (Fig. 15), the interaction of micro architectures with bacterial cell wall and membrane, subsequently damaging the bacterial cell, and an alkaline effect (Qiua et al., 2017 and (Wyszogrodzka et al., 2016). Micro architectures derived antimicrobial agents can be achieved in a simple cost-effective scheme and are appropriate for pronouncing new categories of nano-biotics that could be used as an innovative, ecofriendly, nanoantimicrobial agents. MgO NPs has been used in numerous applications such as catalysis, catalyst supports, toxic waste remediation, refractory materials and adsorbents, additive in heavy fuel oils, reflecting and anti-reflecting coatings, superconducting and ferroelectric thin films as the substrate, superconductors and lithium ion batteries etc. MgO micro architectures also have considerable potential as an antibacterial agent (Wyszogrodzka et al., 2016). Uniquely in presence of micro architectures microbial damage can occurs more rapidly. Accordingly, the biosynthesized MgO micro architectures could have a high potential for use in biological applications. This eco-friendly method of MgO micro architectures synthesis and their application as bactericidal and antifungal agents makes them potential candidates for water treatment, environmental protection, food safety applications, food packaging and biomedical markers.
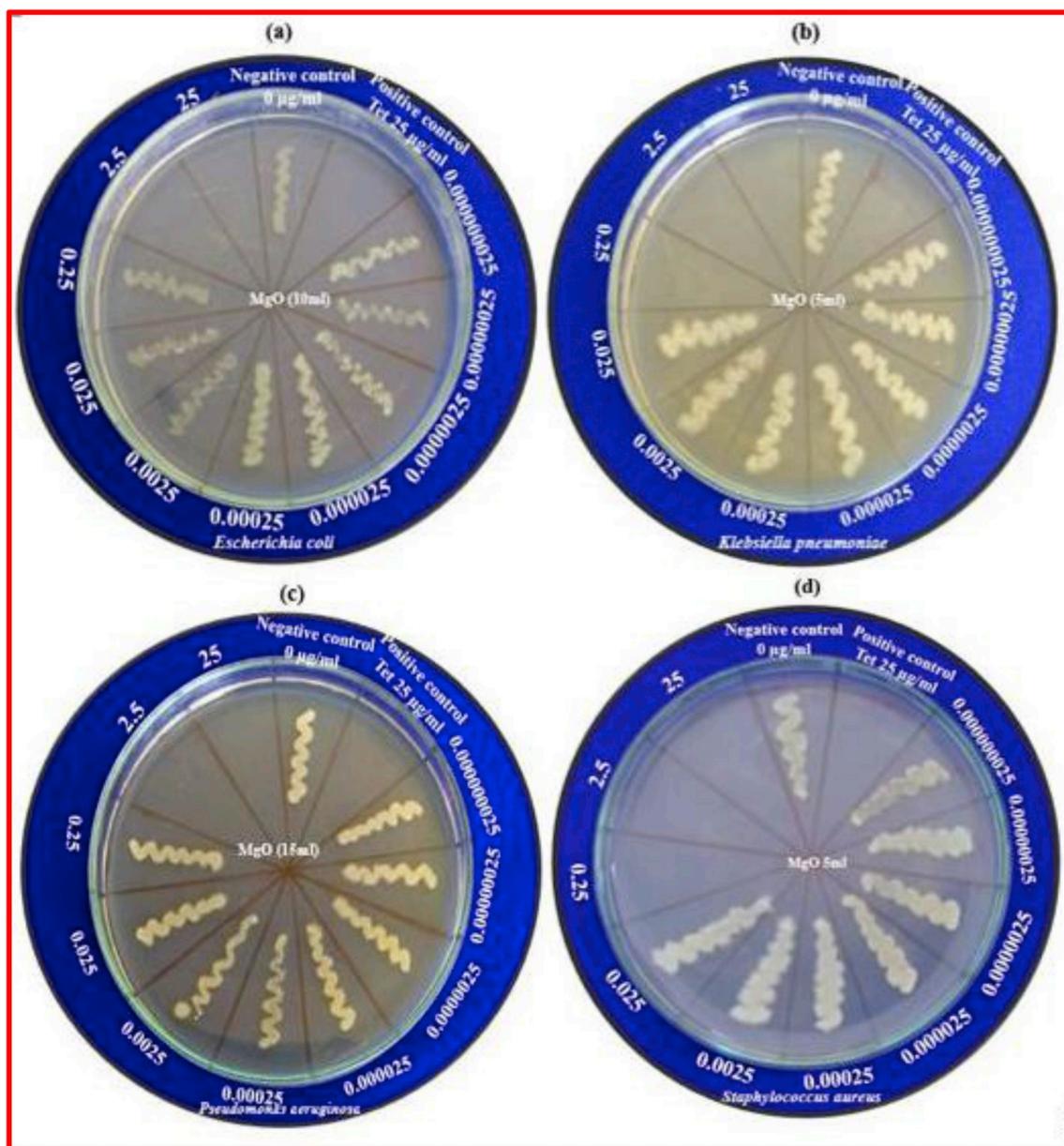
Fig. 13. Antibacterial activity of bioengineered magnesium oxide micro architectures from fruit extract on (a) *E. coli,* (b) *K. pneumonia,* (c) *P. aeruginosa,* (d) *S. aureus.*

4. Conclusions

First time MgO NPs using various concentrations of *Limonia acidissima* fruit extract was synthesized by a simple ecofriendly green combustion. The PXRD patterns of the as-formed products shows single cubic phase without further calcination. The crystallite size was found to be 4–8 nm. The flower like morphology was obtained. The possible growth mechanism was proposed and the trapping of MgO NPs with amino acid Isoleucine was elucidated with egg box model. The diffuse reflectance spectral studies were carried out and energy band gap were estimated between the values 5.06–5.66 eV. PL studies shows excitation spectra at 290 nm and broad emission peak centered at ~395 nm in the bluish-violet region. The CCT value (11289 K) indicated that the NPs can effectively used for fabrication of cool light emitting diodes. The acquired NPs were investigated for their biological activity including antibacterial and antifungal activity. The results designated that MgO NPs were effectively used as good candidates for antibacterial, waste water treatment, food safety applications and biomedical markers.
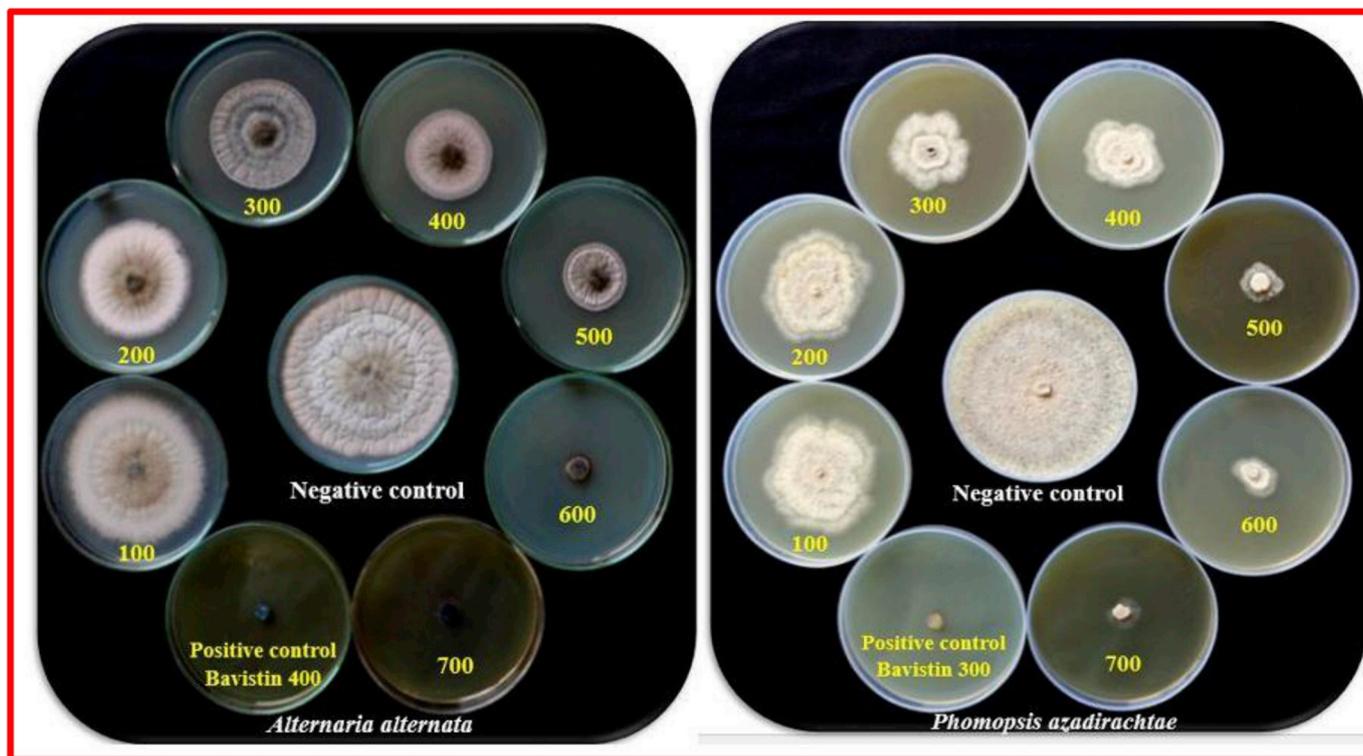
Fig. 14. Growth inhibition of *Phomopsis azadirachtae and Alternaria alternata* by bioengineered magnesium oxide micro architectures.
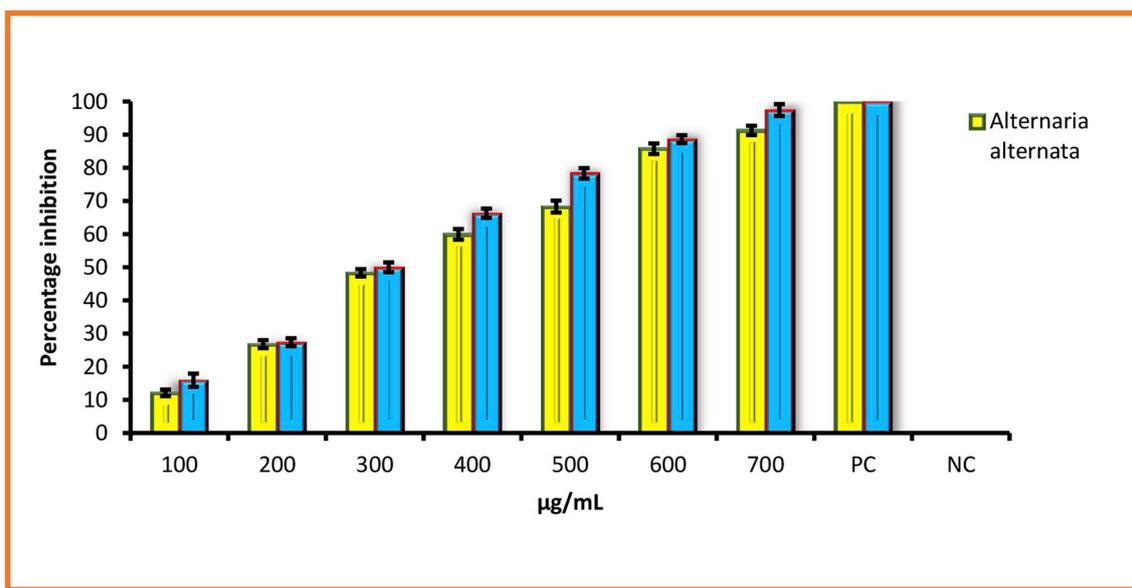

Fig. 15. Antifungal properties of bioengineered magnesium oxide micro architectures on *Alternaria alternata* and *Phomopsis azadirachtae*.
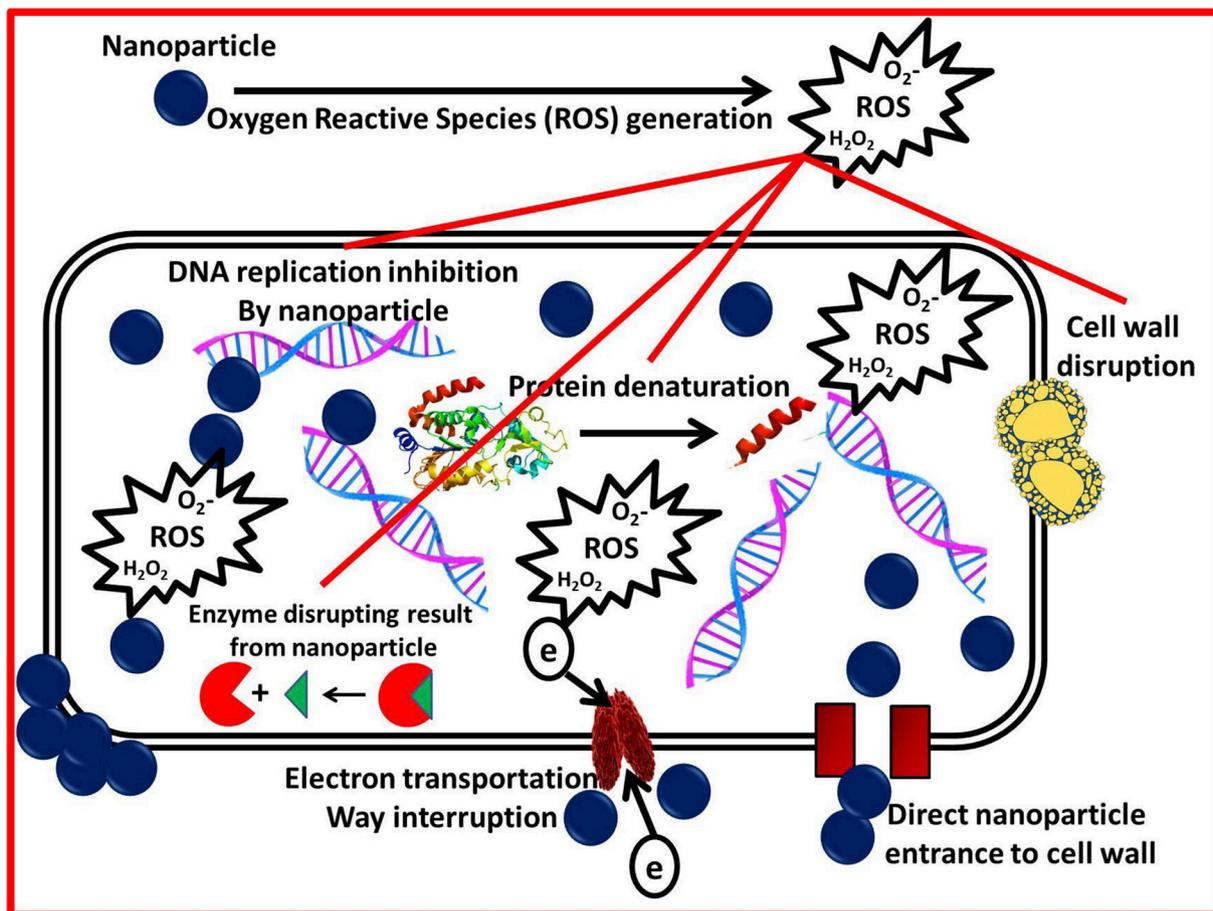
Fig. 16. The multifarious mechanism of bioengineered magnesium oxide micro architectures induced toxicity on pathogenic bacteria. The antimicrobial action such as the formation of ROS, the destruction of cell wall and membrane, and an alkaline effect are involved in death of bacterial cell.

Acknowledgement

Appendix A. Supplementary data

Supplementary data to this article can be found online at https://doi.org/10.1016/j.bcab.2019.01.029.

References

Alhaji, A., Shoja Razavi, R., Ghasemi, A., Loghman-Estarki, M.R., 2017. Modification of Pechini sol–gel process for the synthesis of MgO-Y$_2$O$_3$ composite nanopowder using sucrose-mediated technique. Ceram. Int. 43, 2541–2548.

Aruna, S.T., Mukasyan, A.S., 2008. Combustion synthesis and nanomaterials. Curr. Opin. Solid State Mater. Sci. 12, 44–50.

Bai, J., meng, F., wei, C., zhao, Y., tan, H., liu, J., 2011. Solution combustion synthesis and characteristics of nanoscale MgO powders. Ceramics 55, 20–25.

Basavaraj, R.B., Nagabhushana, H., Daruka Prasad, B., Sharma, S.C., Venkatachalaiah, K.N., 2017a. Mimosa pudica mediated praseodymium substituted calcium silicate nanostructures for white LED application. J. Alloy. Comp. 690, 730–740.

Basavaraj, R.B., Nagabhushana, H., Darshan, G.P., Daruka Prasad, B., Sharma, S.C., Venkatachalaiah, K.N., 2017b. Ultrasound assisted rare earth doped Wollastonite nanopowders: labeling agent for imaging eccrine latent fingerprints and cheiloscopy applications. J. Ind. Eng. Chem. http://doi.org/10.1016/j.jiec.2017.02.019.

Basavaraj, R.B., Nagabhushana, H., Daruka Prasad, B., Vijayakumar, G.R., 2017c. Zinc silicates with tunable morphology by surfactant assisted sonochemical route suitable for NUV excitable white light emitting diodes. Ultrason. Sonochem. 34, 700–712.

Cai, Y., Li, C., Wu, D., Wang, W., Tan, F., Wang, X., Wong, P.K., Qiao, X., 2017. Highly active MgO nanoparticles for simultaneous bacterial inactivation and heavy metal removal from aqueous solution. Chem. Eng. J. 312, 158–166.

Chavan, S.V., Sastry, P.U.M., Tyagi, A.K., 2008. Combustion synthesis of nano-crystalline Nd-doped ceria and Nd$_2$O$_3$ and their fractal behavior as studied by small angle X-ray scattering. J. Alloy. Comp. 456, 51–56.

Chen, L., Sun, X., Liu, Y., Li, Y., 2004. Preparation and characterization of porous MgO and NiO/MgO nanocomposites. Appl. Catal. Gen. 265, 123–128.

Choi, M., Altman, I.S., Kim, Y.J., Pikhitsa, P.V., Lee, S., Park, G.S., Jeong, T., Yoo, J.B., 2004. Formation of shell-shaped carbon micro architectures above a critical laser power in irradiated acetylene. Adv. Mater. 16, 1721–1725.

Devaraja, P.B., Avadhani, D.N., Nagabhushana, H., Prashantha, S.C., Sharma, S.C., Nagabhushana, B.M., Nagaswarupa, H.P., Daruka Prasad, B., 2014a. MgO:Dy^{3+} na-nophosphor: self ignition route, characterization and its photoluminescence proper-ties. Mater. Char. 97, 27–36.

Devaraja, P.B., Avadhani, D.N., Prashantha, S.C., Nagabhushana, H., Sharma, S.C., Nagabhushana, B.M., Nagaswarupa, H.P., 2014b. Synthesis, structural and lumines-cence studies of magnesium oxide nanopowder. Spectrochim. Acta, Part A 118, 847–851.

Devaraja, P.B., Nagabhushana, H., Sharma, S.C., Naik, Ramachandra, Prashantha, S.C., Nagaswarupa, H.P., Anantharaju, K.S., Premkumar, H.B., Jnaneshwara, D.M., 2016. Spectroscopic and photoluminescence properties of MgO:Cr^{3+} nanosheets for WLEDs. Displays 41, 16–24.

Dixit, T., Bilgaiyan, A., Palani, I.A., Nakamura, D., Okada, T., Singh, Vipul, 2015. Influence of potassium permanganate on the anisotropic growth and enhanced UV emission of ZnO nanostructures using hydrothermal process for optoelectronic ap-plications. J. Sol. Gel Sci. Technol. 75, 693–702.

Granados-Correa, F., Bonifacio-Martínez, J., Lara, V.H., Bosch, P., Bulbulian, S., 2008. Cobalt sorption properties of MgO prepared by solution combustion. Appl. Surf. Sci. 254, 4688–4694.

Han, D.Y., Yang, H.Y., Shen, C.B., Zhou, X., Wang, F.H., 2004. Synthesis and size control of NiO micro architectures by water-in-oil microemulsion. Powder Technol. 147, 113–116.

Ianos, R., Lazau, I., 2009. Combustion synthesis, characterization and sintering behavior of magnesium aluminate (MgAl$_2$O$_4$) powders. Mater. Chem. Phys. 115, 645–648.

Jeevanandam, J., Chan, Y.S., Danquah, M.K., 2017. Biosynthesis and characterization of MgO nanoparticles from plant extracts via induced molecular nucleation. New J. Chem. 41, 2800–2814.

Jin, C., Kim, H., Park, S., Lee, C., 2012a. Synthesis of biaxial MgO/Mg–Sn–O nanowire heterostructures and their structural and luminescence properties. J. Alloy. Comp.

541, 163–167.

Jin, C., Kim, H., Park, S., Lee, C., 2012b. Synthesis of biaxial MgO/Mg–Sn–O nanowire heterostructures and their structural and luminescence properties. J. Alloy. Comp. 541, 163–167.

Kaviyarasu, K., Devarajan, P.A., 2011. A versatile route to synthesize MgO nanocrystals by combustion technique. Der Pharma Chem. 3, 248–254.

Kiran, N., Baker, A.P., Wang, G., 2017. Synthesis and luminescence properties of MgO: Sm^{3+} phosphor for white light-emitting diodes. J. Mol. Struct. 1129, 211–215.

Krishnamoorthy, K., Moon, J.Y., Hyun, H.B., Cho, S.K., Kim, S.J., 2012. Mechanistic investigation on the toxicity of MgO micro architectures toward cancer cells. J. Mater. Chem. 22, 24610–24617.

Lakshmeesha, T.R., Sateesh, M.K., Daruka Prasad, B., Sharma, S.C., Kavyashree, D., Chandrasekhar, M., Nagabhushana, H., 2014. Reactivity of crystalline ZnO superstructures against fungi and bacterial pathogens: synthesized using nerium oleander leaf extract. Cryst. Growth Des. 14, 4068–4079.

Mageshwari, K., Mali, S.S., Sathyamoorthy, R., Pati, P.S., 2013. Template-free synthesis of MgO nanoparticles for effective photocatalytic applications. Powder Technol. 249, 456–462.

Medenbach, O., Dettmar, D., Shannon, R.D., Fischer, R.X., Yen, W.M., 2001. Refractive index and optical dispersion of rare earth oxides using a small-prism technique. J. Optic. Pure Appl. Optic. 3, 174–177.

Mirhosseini, M., 2016. Evaluation of antibacterial effect of magnesium oxide micro architectures with nisin and heat in milk. Nanomed. J. 3, 135–142.

Nagabhushana, H., Basavaraj, R.B., Daruka Prasad, B., Sharma, S.C., Premkumar, H.B., Udayabhanu, Vijayakumar, G.R., 2016. Facile EGCG assisted green synthesis of raspberry shaped CdO micro architectures. J. Alloy. Comp. 669, 232–239.

Nassar, M.Y., Mohamed, T.Y., Ahmed, I.S., Samir, I., 2017. MgO nanostructure via a sol-gel combustion synthesis method using different fuels: an efficient nano-adsorbent for the removal of some anionic textile dyes. J. Mol. Liq. 225, 730–740.

Norris, D.J., Efros, A.L., Erwin, S.C., 2008. Doped nanocrystals. Science 319, 1776–1779.

Premkumar, H.B., Sunitha, D.V., Nagabhushana, H., Sharma, S.C., Nagabhushana, B.M., Shivakumara, C., Rao, J.L., Chakradhar, R.P.S., 2013. Synthesis, characterization, EPR, photo and thermoluminescence properties of $YAlO_3$: Ni^{2+} nanophosphors. J. Lumin. 135, 105–112.

Priya Darsini, D.T., Maheshu, V., Vishnupriya, M., Nishaa, S., Sasikumar, J.M., 2016. Antioxidant potential and amino acid analysis of underutilized tropical fruit Limonia acidissima L. Free Radic. Antioxidants. https://doi.org/10.1016/j.fra.2013.08.001.

Qiua, T.A., Meyera, B.M., Christensona, K.G., Klaperb, R.D., Haynes, C.L., 2017. A mechanistic study of TiO_2 nanoparticle toxicity on Shewanella oneidensis MR-1 with UV-containing simulated solar irradiation: bacterial growth, riboflavin secretion, and gene expression. Chemosphere 168, 1158–1168.

Ramakrishna, G., Naik, Ramachandra, Nagabhushana, H., Basavaraj, R.B., Prashantha, S.C., Sharma, S.C., Anantharaju, K.S., 2016. White light emission and energy transfer (Dy^{3+}→ Eu^{3+}) in combustion synthesized YSO: Dy^{3+}, Eu^{3+} nanophosphors. Optik 127, 2939–2945.

Si, R., Zhang, Y.W., You, L.P., Yan, C.H., 2005. Rare-Earth oxide nanopolyhedra, nano-plates, and nanodisks. Angew. Chem. Int. Ed. 44, 3256–3260.

Srivastava, V., Sharma, Y.C., Sillanpaa, M., 2015. Green synthesis of magnesium oxide nanoflower and its application for the removal of divalent metallic species from synthetic wastewater. Ceram. Int. 41, 6702–6709.

Sushma, N.J., Prathyusha, D., Swathi, G., Madhavi, T., Deva Prasad Raju, B., Mallikarjuna, K., Kim, Hak-Sung, 2016. Facile approach to synthesize magnesium oxide nanoparticles by using Clitoria ternatea—characterization and in vitro anti-oxidant studies. Appl. Nanosci. 6, 437–444.

Talebian, N., Amininezhad, S.M., Doudi, M., 2013. Controllable synthesis of ZnO micro architectures and their morphology-dependent antibacterial and optical properties. J. Photochem. Photobiol., B 120, 66–73.

Tamilselvi, P., Yelilarasi, A., Hema, M., Anbarasan, R., 2013. Synthesis of hierarchical structured MgO by sol-gel method. Nano Bull. 2, 130106.

Umesh, B., Eraiah, B., Nagabhushana, H., Sharma, S.C., Nagabhushana, B.M., Shivakumara, C., Rao, J.L., Chakradhar, R.P.S., 2012. Structural, EPR, optical and Raman studies of Nd_2O_3: Cu^{2+} nanophosphors. Spectrochim. Acta, Part A 94, 365–371.

Vasanthia, V., Kottaisamy, M., Anithac, K., Ramakrishnan, V., 2017. Near UV excitable yellow light emitting Zn doped MgO for WLED application. Superlattice. Microst. 106, 174–183.

Wegner, K., Pratsinis, S.E., 2005. Gas-phase synthesis of micro architectures: scale-up and design of flame reactors. Powder Technol. 150, 117–122.

Wyszogrodzka, G., Marszałek, B., Gil, B., Dorożyński, P., 2016. Metal-organic frameworks: mechanisms of antibacterial action and potential applications. Drug Discov. Today 21, 1009–1018.

Yang, S.Y., Kim, S.G., 2004. Characterization of silver and silver/nickel composite particles prepared by spray pyrolysis. Powder Technol. 146, 185–192.

Yang, S., Yi, J.H., Son, S., Jang, J., Altman, I.S., Pikhitsa, P.V., Choi, M., 2003. Fragmentation of Fe_2O_3 micro architectures driven by a phase transition in a flame and their magnetic properties. Appl. Phys. Lett. 83, 4842–4844.

Zawadzki, M., 2008. Microwave-assisted synthesis and characterization of ultrafine neodymium oxide particles. J. Alloy. Comp. 451, 297–300.